

Spatial Confinement of Exciton Transfer and the Role of Conformational Order in Organic Nanoparticles

Dehong Hu,[†] Ji Yu,[‡] G. Padmanaban,[§] S. Ramakrishnan,[§] and Paul F. Barbara^{*†}

Pacific Northwest National Laboratory, P.O. Box 999, Richland, Washington 99352, Department of Chemistry and Biochemistry and the Center for Nano- and Molecular Science and Technology, University of Texas at Austin, Austin, TX 78712, and Department of Inorganic and Physical Chemistry, Indian Institute of Science, Bangalore 560012, India

Received November 5, 2001; Revised Manuscript Received January 31, 2002

ABSTRACT

Organic nanoparticles consisting of single conjugated polymer chains were investigated as a function of degree of conjugation by means of single-molecule spectroscopy. The degree of conjugation was synthetically controlled. For highly conjugated chains, singlet excitons are efficiently funneled over nanometer distances to a small number of sites. In contrast, chains with less conjugation and a high number of saturated bonds do not exhibit energy funneling due to a highly disordered conformation.

This paper is concerned with the spectroscopy of isolated conjugated organic semiconductor nanoparticles, consisting of single conjugated polymer molecules. Single conjugated polymer molecules offer convenient means for obtaining highly conjugated organic nanoparticles. Furthermore, the investigation of single conjugated polymer molecules has led to important insights on the photophysics of conjugated polymers.^{1–6} Organic semiconductor nanoparticles have not been as extensively investigated as their inorganic counterparts, for example, CdSe. For inorganic semiconductors, the optical properties can be tuned over a large range by varying the particle size.^{7,8} This effect is due to quantum confinement of the exciton when the particle size is comparable to or smaller than the exciton Bohr radius R_B . For CdSe, R_B equals 55 Å.⁹ In contrast to the behavior of inorganic semiconductors, organic semiconductors often have an exciton Bohr radius that is about 1 Å, as a result of a much larger carrier effective mass and much smaller dielectric constant,^{10,11} as compared to inorganic semiconductors.⁹ Conjugated organic semiconductors do, however, exhibit a different type of exciton confinement associated with extended one-dimensional π -conjugation.¹² The exciton size for a π -conjugated system is most effectively tuned by chemical alteration of the π -system, i.e., by the introduction of saturated bonds that break the π -conjugation.

Another important property of organic semiconductors that should be sensitive to nanoparticle structure and dimension is the singlet exciton migration length l_s . For example, for the extensively investigated conjugated polymer poly[2-methoxy, 5-(2'-ethyl-hexyloxy)-*p*-phenylene-vinylene] (MEH-PPV), l_s is on the order of 20 nm.¹³ We have recently shown, using single-particle spectroscopy, that certain spectral properties of organic nanoparticles consisting of single MEH-PPV molecules are a consequence of efficient singlet energy transport on a distance scale comparable to the size of the nanoparticles.^{1,3,14} In detail, it was observed that singlet excitons are efficiently “funneled” by energy transfer to a small number of sites in an organic nanoparticle, resulting in red-shifted emission spectra and site-localized photochemistry and photophysics. The surprisingly efficient and directional energy transport (energy funneling) was attributed to a highly ordered conformational structure^{2,4} resulting from conjugated polymer folding within the nanoparticle.

This paper is concerned with the single-molecule spectroscopy and photodynamics of chemical derivatives of MEH-PPV, with broken conjugation due to varying amounts of single-bond defects that replace carbon-carbon double bonds in the phenylene-vinylene backbone, see Figure 1. Using single molecule polarization spectroscopy,^{1,15} the conformational order of a single polymer chain is observed to substantially decrease as the number of single-bond defects are increased synthetically. The polarization spectroscopy experimental results are in reasonable agreement with simulations that employ Monte Carlo calculations for the

* Corresponding author. Fax +1-512-471-3389; email: p.barbara@mail.utexas.edu.

[†] Pacific Northwest National Laboratory.

[‡] University of Texas at Austin.

[§] Indian Institute of Science.

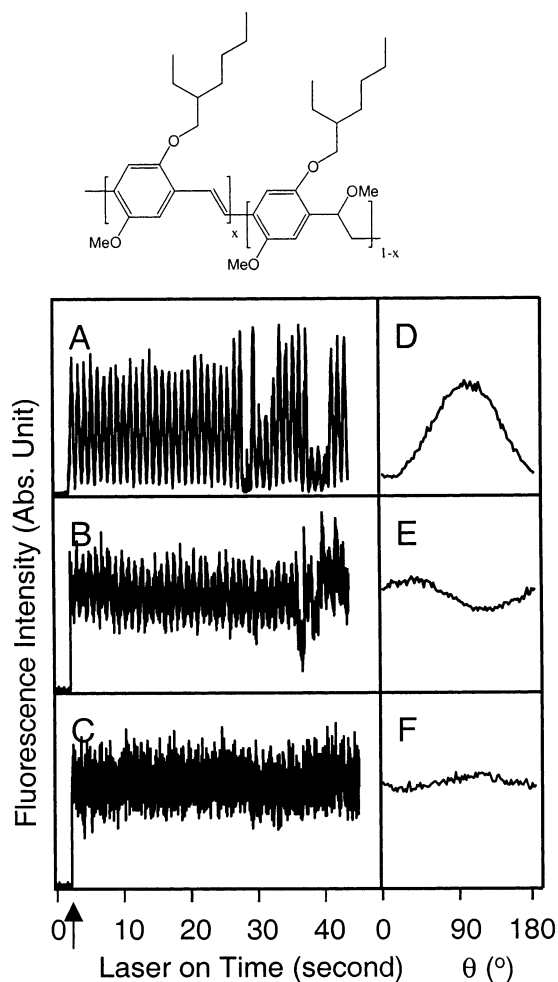


Figure 1. The left panel is the typical single molecule fluorescence intensity transients $I(t)$ of MEH-PPV97 (A), MEH-PPV85 (B), and MEH-PPV45 (C) under linearly polarized excitation with 1 Hz angle spinning. The right panel is the corresponding $I(\theta)$ from averaging the intensity of several cycles of polarization modulation. The structure of MEH-PPV x is shown on the top. The fluorescence signal was collected under continuous wave laser excitation with wavelengths of 457 nm (MEH-PPV45) and 488 nm (MEH-PPV85 and MEH-PPV97).

chain conformations.² The simulations were made as a function of the number of single-bond defects per chain. The single molecule spectroscopy results also demonstrated that the exciton migration length is dramatically reduced in particles with a large number of single-bond defects. This reduction in migration length is manifested by a qualitative reduction in the amount of spectroscopically observed energy funneling.³

The synthetic procedure for two of the samples, MEH-PPV45 and MEH-PPV85, follows the published method¹⁶ that employs a precursor containing methoxy and acetoxy eliminating groups. The polymer samples are denoted by MEH-PPV x , where x is the percentage of C=C double bond. MEH-PPV x contains $x\%$ monomers with vinyl group (C=C double bond) and $(100-x)\%$ monomers with C-C single-bond defects, i.e., with uneliminated methoxy groups (Figure 1). We also studied commercial MEH-PPV (Uniax), denoted by MEH-PPV97. The 97 designation indicates the

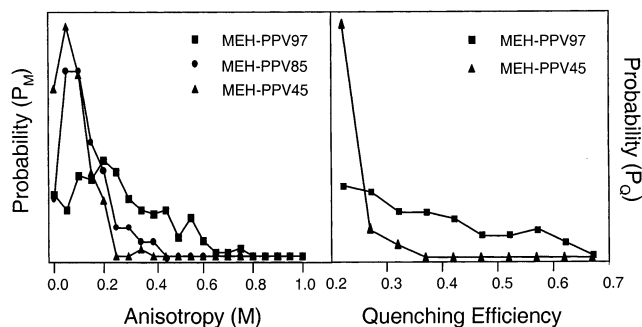


Figure 2. Left: the normalized probability distribution (P_M) of modulation depth (M) for MEH-PPV97, MEH-PPV85, and MEH-PPV45. Right: the probability distribution of quenching efficiency ($Q = 1 - I_{\text{quenched}}/I_{\text{unquenched}}$).

presence of 3% single-bond defects, which was inferred from the wavelength of the absorption maximum (500 nm) of MEH-PPV97 in chloroform solution. The analysis uses a published correlation of absorption maxima vs single-bond defect concentration.¹⁶ The MEH-PPV x samples investigated here have an average molecule weight M_w of 220 000 (for MEH-PPV45 and MEH-PPV85) and 500 000 (for MEH-PPV97). The single molecules were isolated at low concentration in an inert polycarbonate polymer host film on a glass microscope coverslip. The single-molecule microscopy/spectroscopy apparatus and the sample preparation methods have been described previously.³

Figure 1 illustrates the fluorescence intensity transients $I(t)$ for three typical single molecules. Because the direction of polarization (θ) of the linear polarized excitation light is modulated between 0 and π (with a period of one second), $I(t)$ periodically oscillates in time. A time invariant $I(\theta)$ has been determined by time averaging of $I(t)$ synchronized to the modulation period. $I(\theta)$ was fit to the equation²

$$I(\theta) \propto 1 + M \cos 2(\theta - \phi)$$

where the modulation depth M reflects the anisotropy of the excitation ellipsoid projected on the x, y plane (z is the light propagation direction) and ϕ is the angle of maximum intensity for a chosen molecule. $I(\theta)$ represents the angle dependent absorption cross section of the stationary conjugated polymer molecule projected on the x, y laboratory frame.¹⁷

The ensemble probability distributions (P_M) of M for the three MEH-PPV x compounds is important experimental information on the conformation of these compounds (see the left panel of Figure 2). The P_M plots were constructed by measuring the individual M values for more than 100 single molecules and making a histogram of this anisotropy data. The most probable M value and the mean anisotropy \bar{M}_{rms} (Figure 3) are measures of the alignment of the chromophores within a single molecule, assuming the optical transition dipoles of MEH-PPV repeating units are along the chain direction.¹⁸ The experimental results demonstrated that both the most probable M value and \bar{M}_{rms} decrease as the number of single-bond defects increases. For MEH-

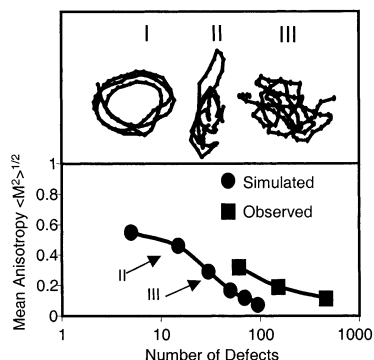


Figure 3. Top: the simulated polymer chain conformation with three different single-bond defect concentrations (I: no single-bond defect, II: 15 single-bond defects per chain, III: 30 single-bond defects per chain). Bottom: the root-mean-square of modulation depth (M) with a series of single-bond defect concentrations of simulated polymer chains (dots) and experimental study of MEH-PPV x single molecules (square). The number of single-bond defects in MEH-PPV x is estimated by the molecular weight M_w and the percentage of defects.

PPV45, the \bar{M}_{rms} is extremely small and close to the measurable limit of our instrument, i.e., $M \leq 0.1$.

It is important to consider the implication of the observed anisotropy data on the conformational structure of the different MEH-PPV x forms. Previous Monte Carlo simulations of polymer chain conformations with few single-bond defects or no defect have shown how \bar{M}_{rms} varies with conformational order and conformational class. \bar{M}_{rms} for MEH-PPV45 is close to Monte Carlo predictions for a disordered conformation, such as a random coil or molten globule conformation. In contrast, the higher \bar{M}_{rms} values for the MEH-PPV with fewer single-bond defect forms according to simulation are indicative of considerably more ordered conformations, such as the toroid (structure I in Figure 3) and defect cylinder (structure II in Figure 3) forms. The toroid and defect cylinder conformations are predicted for stiff conjugated polymers with no single-bond defects and a small number of single-bond defects, respectively.²

This paper presents additional Monte Carlo bead-on-chain simulation results for stiff conjugated polymer chains with random single-bond defects. The chosen parameters for the simulations (chain stiffness, bead-bead attraction energy, and number of beads) are identical to previous simulations of MEH-PPV.^{2,19} Figure 3 presents the average anisotropies (\bar{M}_{rms}) of the simulated conformations as a function of the number of single-bond defects per chain. The simulated results show a trend analogous to the experimental data, i.e., a decrease in anisotropy as the number of single-bond defects increased. The discrepancy between experiment and simulation reflects the oversimplicity of the model, which treats a large portion of the polymer chain (~ 2.5 repeat units) as a single bead. Additionally, the simulations use relatively shorter chains to decrease the computation time and assume a uniform chain length, which also may account for the differences between simulation prediction and the experimental results.

It is interesting to note that for chains with a large fraction of single-bond defects, simulations predict highly disordered

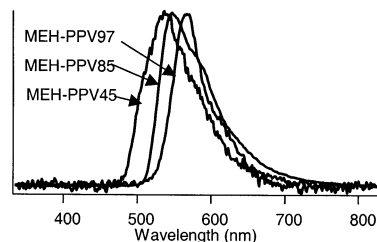


Figure 4. Total fluorescence spectra of ~ 100 single molecules of MEH-PPV97, MEH-PPV85, and MEH-PPV45 in polycarbonate. Excitation wavelength is 457 nm for MEH-PPV45 or 488 nm for MEH-PPV85 and MEH-PPV97.

conformations, such as structure III in Figure 3. This conformation appears to be very similar to the molten globule conformation, which is the stable form of collapsed freely jointed polymer chains. Thus, a large number of single-bond defects “destroys” the conformational order produced by chain stiffness in these simulations and presumably also in real defective MEH-PPV molecules.

The single-molecule spectroscopy data on the MEH-PPV x series offer interesting insights into the spectroscopic and photophysical consequences of conformational disorder for organic nanoparticles. It is well established that an isolated MEH-PPV molecule consists of hundreds of local “quasi-chromophores” along the chain with a distribution of transition energies, each with a length of 10–17 repeat units.²⁰ The distribution is a consequence of conformational distortions,^{4,21} chemical defects,¹⁶ electron correlation effects,²² and chain-chain contacts.²³ To understand the fluorescence spectra of MEH-PPV single molecules, one has to consider two issues: the distribution of transition energies²⁴ and intramolecular electronic energy migration. Ensemble studies on MEH-PPV solutions and thin-film samples suggest that intramolecular electronic energy migration is highly efficient for MEH-PPV with a small number of single-bond defects and results in energy migration over the ~ 20 nm scale in pure films. Energy migration also is responsible for a narrow red-shifted emission spectrum due to energy transfer and subsequent emission from low energy chromophores. In contrast, for MEH-PPV with a large number of single-bond defects, energy migration is much less efficient, resulting in a broadened blue-shifted emission relative to MEH-PPV with a low single-bond defect concentration.¹⁶

Figure 4 shows the first data on the emission spectra of single isolated chains of a conjugated polymer with a large number of single-bond defects. These single-molecule results on the MEH-PPV x series parallel the previously published ensemble measurements.^{16,25} For MEH-PPV97 the narrow red-shifted fluorescence spectrum is highly suggestive of efficient energy migration to a small number of low energy chromophores.¹ Correspondingly, for MEH-PPV45 the single molecule fluorescence spectrum suggests very little energy migration.¹⁶

Additional evidence on how the efficiency of energy migration varies as a function of number of single-bond defects is found in the single molecule intensity fluctuations of the MEH-PPV x series. As discussed in previous pa-

pers,^{1,3,4,14} the single molecule fluorescence intensity of continuously irradiated conjugated polymers exhibits abrupt intensity changes due to the quenching of singlet excitons by reversibly formed, long-lived, photoinjected hole polarons (i.e., radical cations).^{26–28} Examples of this phenomenon are apparent in Figure 1A at 35 and 40 s for MEH–PPV97. The quenching efficiency (fractional drop in intensity) of a single polaron can be nearly 100% for MEH–PPV97 and exhibits a broad distribution, as shown in the right panel of Figure 2. Based on the quenching efficiency, the intramolecular energy migration length of the singlet excitons (which live for ~ 200 ps²⁹) must correspond to a significant portion of the molecule. A typical MEH–PPV molecule is 8 nm in diameter assuming a density of 0.8 g/mL and a MW of 500 000. On the other hand, the quenching efficiency distribution for MEH–PPV45 (Figure 2 right panel) suggests that energy transfer be almost completely suppressed when the number of single-bond defects is significantly increased. This is also apparent in the individual transients as in Figure 1C.

It has been previously been argued that the parallel packing of chain segments in the ordered collapsed defect-cylinder conformation of MEH–PPV97 allows for rapid, directional energy transfer process,³⁰ perhaps by a Förster mechanism. This proposal is supported by the observation that the highly disordered MEH–PPV45 exhibits much less efficient energy migration than the more ordered MEH–PPV97. Another potential reason for less efficient energy migration for MEH–PPV45 may be associated with relatively short average conjugation length of MEH–PPV45 due to the large number of single-bond defects. A short average conjugation length (i.e., number of conjugated C=C bonds) implies a relatively large energy gap between the transition energies of the most probable chromophores. For example, studies on PPV-type oligomers show that for oligomers with a small number of repeat units (2–5) the transition energy varies strongly with the number of repeat units, but for longer oligomers (>7) the transition energy varies much less.²⁰ A larger distribution of energy gaps could, in principle, decrease the rate of Förster energy transfer. Detailed modeling, however, will be necessary to determine whether this latter effect is significant.

In conclusion, energy migration in an MEH–PPV nanoparticle consisting of a single-polymer chain occurs over distances comparable to the particle size and as such is spatially confined by its nanometer dimension. In contrast MEH–PPV nanoparticles with large numbers of single-bond defects do not exhibit nanoscale energy migration or spatial confinement of the energy migration process.

Acknowledgment. This work was supported by grants from the National Science Foundation (P.F.B.) and the Robert A. Welch Foundation. S.R. thanks CSIR, New Delhi, for funding.

References

- (1) Hu, D.; Yu, J.; Barbara, P. F. *J. Am. Chem. Soc.* **1999**, *121*, 6936–6937.
- (2) Hu, D.; Yu, J.; Wong, K.; Bagchi, B.; Rosky, P. J.; Barbara, P. F. *Nature* **2000**, *405*, 1030–1033.
- (3) Yu, J.; Hu, D.; Barbara, P. F. *Science* **2000**, *289*, 1327–1330.
- (4) Huser, T.; Yan, M.; Rothberg, L. J. *Proc. Natl. Acad. Sci. U.S.A.* **2000**, *97*, 11187–11191.
- (5) White, J. D.; Hsu, J. H.; Fann, W. S.; Yang, S.-C.; Pern, G. Y.; Chen, S. A. *Chem. Phys. Lett.* **2001**, *338*, 263–268.
- (6) White, J. D.; Hsu, J. H.; Yang, S.-C.; Fann, W. S.; Pern, G. Y.; Chen, S. A. *J. Chem. Phys.* **2001**, *114*, 3848–3852.
- (7) Li, L.-s.; Hu, J.; Yang, W.; Alivisatos, A. P. *Nano Lett.* **2001**, *1*, 349–351.
- (8) Murray, C. B.; Kagan, C. R.; Bawendi, M. G. *Annu. Rev. Mater. Sci.* **2000**, *30*, 545–610.
- (9) Brus, L. E. *Appl. Phys.* **1991**, *53*, 465.
- (10) The exciton Bohr radius R_B is given by $R_B = 0.53 \text{ \AA} \times \epsilon_r m_e/m^*$ where ϵ_r is the dielectric constant, m^* is effective mass, and m_e is the rest electron mass. Pentacene, for example, $m^* = 1.0 m_e$ and $\epsilon_r = 3$, corresponding R_B is 1.5 Å. See ref 11.
- (11) Schon, J. H.; Kloc, C.; Batlogg, B. *Science* **2000**, *288*, 2338.
- (12) Chandrasekhar, P. *Conducting polymers, fundamentals and applications: a practical approach*; Kluwer Academic: Boston, 1999.
- (13) Savenije, T. J.; Warman, J. M.; Goossens, A. *Chem. Phys. Lett.* **1998**, *287*, 148–153.
- (14) Vanden Bout, D. A.; Yip, W. T.; Hu, D. H.; Fu, D. K.; Swager, T. M.; Barbara, P. F. *Science* **1997**, *277*, 1074–1077.
- (15) Ha, T.; Laurence, T. A.; Chemla, D. S.; Weiss, S. J. *J. Phys. Chem. B* **1999**, *103*, 6839–6850.
- (16) Padmanaban, G.; Ramakrishnan, S. *J. Am. Chem. Soc.* **2000**, *122*, 2244–2251.
- (17) Thulstrup, E. W.; Michl, J. *Elementary Polarization Spectroscopy*; VCH: New York, 1989.
- (18) Hagler, T. W.; Pakbaz, K.; Heeger, A. J. *Phys. Rev. B* **1994**, *49*, 10968–10975.
- (19) All simulations were conducted on the same cubic three-dimensional lattice by bond fluctuation method. The lattice constant is 0.3 nm. The linked bead distance is restricted from 1.2 to 1.8 nm (4 to 6 lattice units). The bead displacement is one lattice unit. The chain length is 100 beads. The attraction energy is the Lennard-Jones potential with a depth of 0.6 kT and the chain stiffness is 10 kT rad⁻².
- (20) Woo, H. S.; Lhost, O.; Graham, S. C.; Bradley, D. D. C.; Friend, R. H.; Quattrecchi, C.; Bredas, J. L.; Schenk, R.; Mullen, K. *Synth. Met.* **1993**, *59*, 13–28.
- (21) Yaliraki, S. N.; Silbey, R. J. *J. Chem. Phys.* **1996**, *104*, 1245–1253.
- (22) Mukamel, S.; Tretiak, S.; Wagersreiter, T.; Chernyak, V. *Science* **1997**, *277*, 781–787.
- (23) Nguyen, T. Q.; Doan, V.; Schwartz, B. J. *J. Chem. Phys.* **1999**, *110*, 4068–4078.
- (24) Bassler, H.; Schweitzer, B. *Acc. Chem. Res.* **1999**, *32*, 173–182.
- (25) Manoj, A. G.; Narayan, K. S.; Gowri, R.; Ramakrishnan, S. *Synth. Met.* **1999**, *101*, 255–256.
- (26) Orion, I.; Buisson, J. P.; Lefrant, S. *Phys. Rev. B* **1998**, *57*, 7050–7065.
- (27) Abdou, M. S. A.; Orfino, F. P.; Son, Y.; Holdcroft, S. *J. Am. Chem. Soc.* **1996**, *119*, 4518–4524.
- (28) McNeill, J. D.; O'Connor, D. B.; Adams, D.; Barbara, P. F.; Kämmer, S. B. *J. Phys. Chem. B* **2001**, *105*, 76–82.
- (29) Hayes, G. R.; Samuel, I. D. W.; Phillips, R. T. *Phys. Rev. B* **1995**, *52*, 11569–11572.
- (30) Nguyen, T. Q.; Wu, J. J.; Doan, V.; Schwartz, B. J.; Tolbert, S. H. *Science* **2000**, *288*, 652–656.

NL0156610